This is the author-manuscript version of this work - accessed from http://eprints.qut.edu.au

Adam, Clayton J. and Loughran, Jeffrey G. (2007) Finite element prediction of the performance of sugarcane rolling mills. *International Sugar Journal* 109(1301):pp. 272-284.

Copyright 2007 Clayton J. & Jeffrey G. Loughran

Optimising the Design of Sugarcane Rolling Mills using Finite Element Computer Simulation

C.J. Adam[1]; J.G. Loughran[2]

[1]School of Engineering Systems, Queensland University of Technology, GPO Box 2434, Brisbane, Q4001, Australia; e-mail of corresponding author: c.adam@qut.edu.au

[2]School of Engineering, James Cook University, Townsville, Q4811, Australia; e-mail: jeffrey.loughran@jcu.edu.au

Abstract

Extraction of juice from shredded sugarcane is commonly performed using sets of counter-rotating rolls. The design of sugarcane rolling mills is largely based on previous experience, and increases in crushing rate through factory mills have therefore been achieved by increasing blanket thickness rather than roll surface speed due to concerns regarding loss of extraction efficiency at higher rolling speeds. Estimation of roll loads, torques and expected juice extraction for a given mill design has likewise been empirical, with limited consideration of the underlying physical processes governing mill performance.

The advent of finite element simulation techniques and increases in computing power have provided new tools to simulate and optimise rolling mill performance however. This study applies finite element methods to solve the governing mathematical equations for flow of juice through the fibrous sugarcane blanket and to predict roll load and torque, extraction energy, frictional sliding on the roll surface, and the behaviour of roll grooves during crushing. Our results to date suggest that higher roll speeds and thinner blankets (than those currently used in industry practice) would maintain crushing rates and juice extraction levels while reducing roll load, torque, and power

consumption, and decreasing frictional sliding between rolls and cane blanket.

Notation

a,b,c	coefficients in permeability relation
d	cohesion in Drucker-Prager material model
C	mill compression ratio
D	roll diameter
$\boldsymbol{D_T}$	constitutive tangent matrix
e	void ratio
$\mathrm{F_{cone}}$	cone yield surface in Drucker-Prager plasticity model
$\mathrm{F_{cap}}$	cap yield surface in Drucker-Prager plasticity model
$\mathrm{G_{cone}}$	cone flow potential in Drucker-Prager plasticity model
G_α	included angle of grooves in friction coefficient relation
h_0	reference blanket thickness for two-roll mill
h_{ng}	no-gas (saturated) thickness of cane blanket
$\boldsymbol{I}$	identity matrix
k	intrinsic permeability
$\boldsymbol{K}$	permeability coefficient matrix
$\boldsymbol{L}$	differential operator
$\boldsymbol{m}$	trace operator
$\boldsymbol{v}$	pore fluid velocity
p	first stress invariant (hydrostatic)
p_a	evolution parameter in Drucker-Prager plasticity model
p_b	initial cap size in Drucker-Prager plasticity model
P	pore fluid pressure
∇P	fluid pressure gradient
q	second stress invariant (deviatoric)
R	cap eccentricity in Drucker-Prager material model
S	roll surface speed
$\boldsymbol{S}$	deviatoric stress tensor
S_r	relative rubbing speed in friction coefficient relation
$\boldsymbol{u}$	displacement vector
α	smoothing parameter in Drucker-Prager material model
β	friction angle in Drucker-Prager material model
$\boldsymbol{\varepsilon}$	strain tensor
$\dot{\boldsymbol{\varepsilon}}$	mechanical strain rate
μ	friction coefficient
$\boldsymbol{\sigma}$	total stress tensor
$\boldsymbol{\sigma'}$	effective stress tensor
σ_n	normal contact pressure in friction coefficient relation

1. Introduction

Sugarcane is a grass of the genus *Saccharum* which is grown throughout tropical and subtropical regions, producing approximately 94 million tonnes of raw sugar worldwide in 2003/2004 (USDA, 2004). Factory processing of sugarcane begins with shredding and crushing of harvested cane stalks to extract the sucrose-containing juice. Mechanical expression of juice from prepared sugarcane is commonly performed using sets of counter rotating rolls. The rolling process is energy intensive and must obtain a high degree of liquid extraction without compromising processing rate.

Sugar factories have undergone dramatic increases in processing rate over the past five decades, and this has been largely achieved by increasing blanket thickness through existing equipment without much change in the rotational speed of the rolls. Roll surface speeds above 300 mm/s have been avoided since they are traditionally associated with decreased extraction efficiency (Bullock, 1957). However, recent factory experience with two-roll mills operating at higher surface speeds suggests that good performance can be achieved at roll surface speeds up to at least 400 mm/s in the presence of adequate juice drainage.

If increased throughput is possible using either thicker blankets or higher roll speeds without compromising extraction efficiency, the preferred approach should be determined with reference to the energy required, as well as the potential wear-related maintenance costs associated with higher speed thin blankets versus lower speed thick blankets.

Previous milling investigations (Crawford, 1955; Bullock, 1957; Murry, 1960; Braddock, 1963; Cullen, 1965; Holt, 1967; Solomon, 1967; Murry & Holt, 1967) have established a sound theoretical basis for volumetric juice extraction by rolling, however the prediction of actual milling unit performance was largely empirical from 1960-1990, with limited consideration of internal and interfacial cane blanket conditions during rolling. Subsequent increases in computing power and development of finite element algorithms led to advanced computational simulations of the sugar

cane crushing process (Loughran, 1990; Zhao, 1993; Adam, 1997; Downing, 1999; Kent, 2003; Kannapiran, 2003).

This study uses mathematical modelling of the sugar cane crushing process to investigate the effect of blanket thickness on extraction energy in sugarcane crushing mills.

2. Methodology

The mathematical model is implemented using the finite element (FE) method, and model parameters are calibrated using experimental data for the constitutive behaviour of prepared sugar cane reported by previous researchers. FE models are well suited to investigation of the crushing process, as they allow simulation of non-linear porous material behaviour, together with coupled fluid flow through porous media such as occurs in the cane blanket during juice expression by rolling.

2.1. *Governing equations*

Physically, the shredded sugar cane (*Fig. 1*) comprises a porous fibrous solid matrix surrounded by juice and air in the interstices between fibres. The solid phase is distributed throughout the medium, and the voids form an overlapping continuum.

Application of porous media mechanics theory to the rolling of prepared sugar cane is simplified by the following assumptions.

(1) Dynamic effects are negligible (quasi-static).

(2) Gravitational effects are negligible.

(3) The medium is fully saturated.

(4) Bulk incompressibility of solid and liquid phases.

(5) Terzaghi's principle of effective stress is valid.

(6) Darcy's law is valid.

For these conditions, the governing equations are expressed as follows (Owen *et al*. 1995). Darcy's law relates the pore fluid flow velocity $\boldsymbol{v}$ in m/s to the pressure gradient ∇P in Pa *via* the permeability coefficient matrix $\boldsymbol{K}$ (assumed isotropic),

$$\boldsymbol{v} = \boldsymbol{K}\nabla P \tag{1}$$

The overall equilibrium equation for the porous medium is written as:

$$\boldsymbol{L}^{\mathrm{T}}\boldsymbol{\sigma} = 0 \tag{2}$$

where: $\boldsymbol{L}$ is the differential operator; T is the transpose operator and $\boldsymbol{\sigma}$ is the total stress tensor. The continuity equation for the wetting liquid is written in terms of the pore fluid velocity $\boldsymbol{v}$ and mechanical strain rate $\dot{\boldsymbol{\varepsilon}}$ as:

$$-\nabla^{\mathrm{T}}\boldsymbol{v} = \boldsymbol{m}^{\mathrm{T}}\dot{\boldsymbol{\varepsilon}} \tag{3}$$

where the gradient operator ∇ is:

$$\nabla^{\mathrm{T}} = \left[\frac{\partial}{\partial x}, \frac{\partial}{\partial y}, \frac{\partial}{\partial z}\right]$$

and the transpose of the trace operator $\boldsymbol{m}^{\mathrm{T}}$ is:

$$\boldsymbol{m}^{\mathrm{T}} = [1,1,1,0,0,0]$$

Terzaghi's principle of effective stress relates the effective stress $\boldsymbol{\sigma}'$ acting on the solid matrix to the total stress $\boldsymbol{\sigma}$ and pore pressure P

$$\boldsymbol{\sigma} = \boldsymbol{\sigma}' - \boldsymbol{m}P \qquad (4)$$

The system of equations is completed by specification of a constitutive relation for the solid matrix relating changes in effective stress $\mathrm{d}\boldsymbol{\sigma}'$ to incremental strains $\mathrm{d}\boldsymbol{\varepsilon}$ *via* the tangent matrix $\boldsymbol{D}_T$;

$$\mathrm{d}\boldsymbol{\sigma}' = \boldsymbol{D}_T \mathrm{d}\boldsymbol{\varepsilon} \qquad (5)$$

In addition, the incremental strain-displacement relation is defined as

$$\mathrm{d}\boldsymbol{\varepsilon} = \boldsymbol{L}^{\mathrm{T}} \mathrm{d}\boldsymbol{u} \qquad (6)$$

where $\mathrm{d}\boldsymbol{u}$ represents the incremental displacement vector.

2.2. *Numerical solution schemes*

The system of governing equations is solved using the finite element method. Spatial and temporal discretisation is followed by non linear equation solution and integration of the elasto-plastic constitutive equations for the solid matrix (deSouza Neto *et al.* 1997).

2.3. *Constitutive parameters*

Having defined the theoretical basis for analysis of the rolling problem, both permeability and constitutive relations must be defined over the full range of conditions to be simulated. In addition, frictional behaviour at the interface between rolls and the cane blanket must be prescribed.

2.3.1. *Solid phase*

As previously stated, the solid matrix of prepared sugar cane is comprised of discrete fibrous particles, initially loosely arranged. Application of compressive stress results in frictional sliding,

reorientation, and bending of the fibres orthogonal to the direction of applied stress. Observed features of the solid matrix constitutive response are:

(1) highly compressible, yields under hydrostatic pressure;
(2) exhibits large plastic volume strains;
(3) non linear plastic strain hardening and non linear elastic recovery during compression/relaxation;
(4) plastic strains in uniaxial compression that are largely co-directional with applied stress, little transverse deformation;
(5) small tensile strength;
(6) anisotropic behaviour due to layering of fibres; and
(7) no shear failure occurring during uniaxial or triaxial compression.

Of these features, material anisotropy is neglected due to the complexity involved in formulation and calibration of anisotropic plasticity models. In addition, simple linear elastic material behaviour is assumed initially, since subsequent plastic deformation dominates the material response during rolling. The additive strain rate decomposition is given by:

$$\mathrm{d}\varepsilon = \mathrm{d}\varepsilon^{el} + \mathrm{d}\varepsilon^{pl} \qquad (7)$$

where ε^{el} and ε^{pl} respectively are the elastic and plastic components of total strain ε.

A modified isotropic (capped) Drucker-Prager plasticity relation is chosen to represent the inelastic component of fibrous matrix deformation (Drucker & Prager, 1952). The yield surface and plastic flow potential are both shown in *Fig. 2*. The isotropic yield surface comprises a ‘cone’ or shear failure surface, and a ‘cap’ which provides pressure dependent yield. Strain hardening or softening of the cap is controlled by plastic volumetric strain, while the cone yield surface is fixed. The cap

and cone are joined smoothly using a small segment of transition yield surface. Associated flow is assumed on the cap, and elliptical non-associated flow on the cone and transition regions.

Assuming rotational symmetry in the $\prod$ plane, the yield surface may be expressed completely in terms of the first and second stress invariants, p and q, defined as,

$$p = -\frac{1}{3} trace(\boldsymbol{\sigma}') \tag{8}$$

$$q = \sqrt{\frac{3}{2}\boldsymbol{S} : \boldsymbol{S}} \tag{9}$$

$$\boldsymbol{S} = \boldsymbol{\sigma}' + p\boldsymbol{I} \tag{10}$$

where $\boldsymbol{S}$ is the deviatoric stress tensor and $\boldsymbol{I}$ is the identity matrix. Yield surface and flow potential equations for the capped Drucker-Prager plasticity model are then given in Eqns (11) to (13), where F_{cone} is the cone yield surface, F_{cap} is the cap yield surface, G_{cone} is the plastic flow potential on the cone, β is the friction angle, d is the cohesion, R is the cap eccentricity, and α is a smoothing parameter defining the size of the transition region.

$$F_{cone} = q - p\tan\beta = 0 \tag{11}$$

$$F_{cap} = \sqrt{(p - p_a)^2 + \left[\frac{Rq}{(1 + \alpha - \alpha/\cos\beta)}\right]^2} - R(d + p_a \tan\beta) = 0 \tag{12}$$

$$G_{cone} = \sqrt{[(p - p_a)\tan\beta]^2 + \left[\frac{q}{1 + \alpha - \alpha/\cos\beta}\right]^2} \tag{13}$$

The evolution parameter p_a is defined as

$$p_a = \frac{p_b - Rd}{(1 + R\tan\beta)} \tag{14}$$

where p_b is the initial size of the cap in the Drucker-Prager model. Material properties for the isotropic linear elasticity and capped Drucker-Prager plasticity models were determined using a combination of direct experimental measurement and inverse calibration from uniaxial, confined uniaxial, and triaxial compression experiments (Leitch, 1996; Adam, 1997).

2.3.2. *Liquid flow*

Flow of liquid through the fibrous solid matrix is described *via* Darcy's law. The intrinsic permeability k is assumed dependent on void ratio only, where void ratio e is the ratio of voids volume to volume of solid material. Experimental measurements of the permeability response exhibit a strongly non-linear decrease of permeability with decreasing void ratio, described as

$$k = a\left(\frac{c}{1+e}\right)^{-b} \tag{15}$$

where coefficients a, b, and c depend on the fineness of preparation and fibre content of the material. The permeability response used for finite element simulation is shown in *Fig. 3*, and includes a modification for seepage-induced consolidation during flow cell permeability experiments, and flow in regions which may be partially saturated (Adam & Loughran, 2004a).

2.3.3. *Interfacial friction*

Direct experimental measurements of the friction coefficient between prepared cane and metal surfaces indicate that friction decreases with increasing normal pressure and increasing relative rubbing speed at the roll/blanket interface. Circumferential roll grooves tend to increase the

effective friction coefficient due to wedging of material between the grooves, with narrower included grooving angles enhancing effective friction coefficient. Multi linear regression of available data yields the frictional relation used for finite element analysis (Adam & Loughran, 2004b),

$$\mu = 1 - 8.7\times10^{-2}\ln(\sigma_n) - 2.2\times10^{-3}S_r - 1.3\times10^{-3}G_\alpha + 8.0\times10^{-5}\ln(\sigma_n)G_\alpha + 2.7\times10^{-4}\ln(\sigma_n)S_r \quad (16)$$

where μ is the friction coefficient, σ_n is the normal pressure across the roll/blanket interface in kPa, S_r is the relative rubbing speed across the roll/blanket interface in mm/s, and G_α is the included angle of circumferential roll grooves in degrees.

2.4. *Implementation in a two-roll mill Finite Element model*

Figure 4 shows a schematic representation of a two-roll mill. The compression ratio *C* for a two-roll mill is defined as the ratio of the no-gas (fully saturated) volume of material entering the mill per unit time to the escribed volume (nip length × height × speed) of the mill.

Symmetry is utilised to model only half of the cane blanket, and variations in the axial direction of the rolls are neglected, allowing two-dimensional plane strain analysis. Rolls are assumed rigid and fully permeable (free-draining). Lagrangian finite element solution is performed, so that the mesh moves with and is attached to the solid material. The solution progresses until steady state values for roll load, torque, and liquid pressure distribution within the blanket are achieved. The FE solutions for this study were performed using the ABAQUS/Standard software (v6.2, Abaqus Inc, RI, USA).

2.5. *Extraction energy*

The work of deformation for a saturated porous material may be divided into two components; (a) work related to bulk deformation of the fibrous solid matrix, and (b) work related to juice flow

through the fibrous solid matrix, which includes seepage induced consolidation (deformation of the solid phase due to liquid pressure gradients within the material). For the continuous process of cane crushing however, extraction energy may be further categorised so that total external energy is dissipated internally by one of four mechanisms:

(1) *bulk plasticity* - energy dissipated through plastic straining of the fibrous solid matrix, with bulk plasticity solely related to the overall solid matrix deformation occuring during rolling and excluding the effects of juice flow;

(2) *frictional sliding* - energy dissipated due to frictional sliding at the roll/blanket interface;

(3) *juice flow* - energy dissipated due to juice flow through the pores of the fibrous solid matrix; and

(4) *seepage induced plasticity* - energy dissipated through seepage-induced plastic straining of the fibrous solid matrix.

Note that of the total solid matrix deformation, only plastic strains contribute to internal energy dissipation since elastic strains are recoverable during elastic unloading of the cane blanket. Since the rolling process is continuous, predicted energy dissipation components are expressed in terms of energy per unit crushing rate, kWh/t [cane].

3. Results and discussion

Figures 5 and *6* compare predicted and experimental (Loughran, 1990) roll load and torque *versus* nip compression ratio. Finite element results for two sets of material properties are shown, where each set was based on different compression test data. Set 1 material properties were determined from very low speed (5 and 10mm/min) compression tests on Q96 variety sugar cane. Set 2 material properties were determined by extrapolation to determine the zero-speed (solid matrix

only) component from tests performed at higher compression speed (18-71mm/s), using coarser (less finely shredded) cane samples. The two sets are representative of variations in cane blanket properties which may occur in factory milling due to variations in cane variety and level of comminution. In both cases, predicted trends are in good agreement with experiment, while levels depend on the cane variety, fibre content, and fineness of preparation used for determination of material parameters. The use of two-dimensional analysis tends to underestimate roll torques since the roll grooves introduce shearing stresses which are not accounted for in plane strain simulation, however the FE models provide a valid and useful tool for comparative assessment of different rolling mill configurations.

3.1. *Effect of compression ratio, speed, diameter and blanket thickness*

Figure 7 shows the predicted specific power components for each energy dissipation mechanism as a function of nip compression ratio for the two-roll mill simulations. *Figures 8 and 9* give variations in extraction energy with roll surface speed and blanket thickness respectively.

With reference to *Fig. 7*, the power required for bulk plastic deformation increases with mill compression ratio as expected. No energy dissipation occurs due to frictional sliding at the roll/blanket interface until a compression ratio of about 2.5. At a nip compression ratio of 3.0 however, frictional sliding on the roll surface accounts for approximately 20% of total power consumption. This significant proportion of crushing energy is not useful for juice extraction, and is the primary contributor to roll wear during crushing. Energy dissipation due to juice flow and seepage induced plasticity also increases with compression ratio, with the combined effects accounting for 40-45% of total crushing energy at compression ratios of 2.5-3.0.

With reference to *Fig. 8*, increasing roll surface speed has no effect on bulk plasticity since nip compression ratio and overall blanket deformation both remain constant. Frictional energy dissipation has no effect until roll surface speeds of approximately 150 mm/s, beyond which frictional sliding accounts for an increasing proportion of total energy consumption. The juice flow component of energy consumption decreases slightly with increasing roll surface speed rather than

increasing as expected from simple flow considerations. However, this behaviour is a direct consequence of the pressure limiting extrusion mechanism known as *reabsorption* (Murry, 1960; Murry & Holt, 1967), and is reflected by the increase in seepage induced plasticity with increasing roll surface speed. Note that total specific power consumption increases with increasing roll surface speed, suggesting that increasing roll surface speed without any reduction in blanket thickness will decrease energy efficiency.

With reference to *Fig. 9*, overall energy consumption decreases with decreasing blanket thickness. Energy dissipation due to frictional sliding and seepage induced plasticity are the main contributors in the overall trend, although bulk plasticity also decreases very slightly for thinner blankets. The decrease in frictional sliding energy is primarily a result of the reduced contact angles obtained with thinner blankets. Reducing blanket thickness also increases the frictional roll surface constraint on material in the nip region, accounting for the observed decrease in seepage induced consolidation.

3.2. *Effect of blanket thickness at constant crushing rate*

Although *Figs. 7* to *9* provide a useful indication of the key variables affecting extraction energy, they do not represent practical milling situations since crushing rate is not maintained (for example in *Fig. 9*, reducing blanket thickness while roll surface speed remains constant would reduce the crushing rate through the mill). *Figure 10* shows deformed finite element meshes for a series of simulations in which the blanket thickness was varied from 25-100% of the benchmark value h_0 while altering roll surface speed to maintain constant crushing rate. The roll nip opening was also altered to maintain constant compression ratio (corresponding to approximately constant juice extraction).

The blanket thickness, roll speed, and predicted results of these simulations are given in Table 1, and show a substantial decrease in both roll load and torque with decreasing blanket thickness. This result is to be expected since decreasing blanket thickness decreases the contact area of material on the rolls. Maximum juice pressures remained approximately constant due to the

increase in roll speed. Predicted juice extractions are not shown, but increased slightly with decreasing blanket thickness. Predicted power requirements (roll torque times rotational velocity) decrease by nearly 30% with decreasing blanket thickness.

These results suggest that decreasing blanket thickness while increasing roll surface speed to maintain crushing rate will result in slight increases in extraction performance as well as significantly lower roll loads, torques, and power consumption. Further, reduced frictional sliding between rolls and cane blanket should lead to reduced maintenance costs due to roll wear. Although mill feeding behaviour was not considered explicitly in this study, the smaller contact angles associated with reduced blanket thickness would also be expected to augment mill feeding performance.

As mentioned in the introduction, recent experience in factory mills has shown that good juice extractions can be achieved with higher roll surface speeds than previously thought, provided that adequate juice drainage paths exist. This study provides a theoretical confirmation of such experience and points to the need for further experimentation to fully investigate the potential advantages of high speed, thin blanket sugarcane milling.

4. Conclusions

Energy dissipation during rolling of prepared sugarcane can be characterised in terms of four components; bulk plasticity, frictional sliding, juice flow, and seepage induced plasticity. Finite element simulations of a two-roll mill predict that frictional sliding does not occur until nip compression ratios of approximately 2.5 and roll surface speeds of 150 mm/s. At high compression ratios with normal blanket thickness, frictional sliding on the roll surface can comprise up to 20% of total power consumption, with significant implications for roll wear. Constant crushing rate simulations suggest that thinner blankets and higher roll speeds will reduce frictional sliding, roll load and torque, power requirements, and slightly improve juice extraction.

5. Acknowledgements

The authors wish to thank the Australian Sugar Research and Development Corporation for their support of this investigation.

References

Adam C J (1997). Application of computational porous media mechanics to the rolling of prepared sugar cane. PhD Thesis, James Cook University, Australia

Adam C J; Loughran J G (2004a). Seepage induced consolidation in permeability measurements for fibrous porous media – a finite element investigation. Journal of Porous Media, **7**(2),101-117

Adam C J; Loughran J G (2004b). Multi-variate analysis of frictional interaction between grooved roller and prepared sugarcane. Transactions of the American Society of Agricultural Engineers, **47**(5),1611-18

Braddock T E (1963). The coefficient of friction between prepared cane and metal surfaces. BE Thesis, University of Queensland, Australia

Bullock K J (1957). An investigation into the crushing and physical properties of sugar cane and bagasse. PhD Thesis, University of Queensland, Australia

Crawford W R (1955). Mill feeding – the basic factor in efficient cane milling. Proc Qld Soc of Sugar Cane Tech, 167-79

Cullen R N (1965). An investigation of the shear strength of bagasse. MEngSc Thesis, University of Queensland, Australia

DeSouza Neto E A; Zhao S Y; Owen, D R J; Peric D; Loughran J G (1997). Finite element simulation of the rolling of multi-phase materials. Computational Plasticity, Fundamentals and Applications, **5**,1296-1304

Downing C M (1999). Investigation of the effects of soil contamination on the crushing of comminuted sugar cane. PhD Thesis, James Cook University, Australia

Drucker D C; Prager W (1952). Soil mechanics and plastic analysis or limit design. Quarterly of Applied Mathematics, **10**(2),157-165

Holt J E (1963). The prediction of roll loads in the crushing of prepared sugar cane. MEng Thesis, University of Queensland, Australia

Kannapiran A (2003). Computational and experimental modeling of the crushing of prepared sugar cane. PhD thesis, James Cook University, Australia

Kent G A (2003). Increasing the capacity of Australian raw sugar factory milling units. PhD thesis, James Cook University, Australia

Leitch C J (1996). An experimental investigation into the constitutive behaviour of prepared sugar cane. MSc Thesis, James Cook University, Australia

Loughran J G (1990). Mathematical and experimental modeling of the crushing of prepared sugar cane. PhD Thesis, University of Queensland, Australia

Murry C R (1960). The mechanics of crushing prepared sugar cane. PhD thesis, University of Queensland, Australia

Murry C R; Holt JE (1967). The mechanics of crushing sugar cane. Elsevier. Amsterdam

Owen D R J; Zhao S Y; Loughran J G (1995). Application of porous media mechanics to the numerical solution of the rolling of prepared sugar cane. Engineering Computations, **12**(3),281-302

Solomon T J (1967). Theoretical and experimental studies in the mechanics of crushing sugar cane. University of Queensland, Australia, PhD Thesis

USDA (2004). World production, supply and distribution – centrifugal sugar. United States Department of Agriculture, Washington DC. http://www.fas.usda.gov/htp/sugar/2004/June%202004%20PSD.pdf (access date 28 Oct 2004)

Zhao S Y (1993). Finite element solution of saturated-unsaturated porous materials with application to the rolling of prepared sugar cane. PhD thesis, University College of Swansea, Wales

Figure captions

Fig. 1. Structure of shredded sugar cane

Fig. 2. Yield surface and flow potential for capped Drucker-Prager plasticity: d, cohesion; β, friction angle; α, cap smoothing parameter; p_a, initial cap size; p_b, current cap size

Fig. 3. Permeability response for finite element simulation: ⊟, directly measured; ⊖, modified

Fig. 4. Schematic two-roll mill

Fig. 5. Roll load versus compression ratio for experiment and finite element simulation: ---□-- empirical (Loughran, 1990), —◇— simulation (set 1 material parameters), —●— simulation (set 2 material parameters). Set 1 material properties were determined from very low speed (5 and 10mm/min) compression tests on Q96 variety sugar cane. Set 2 material properties were determined by extrapolation to determine the zero-speed (solid matrix only) component from tests performed at higher compression speed (18-71mm/s), using coarser (less finely shredded) cane samples. The two sets are representative of variations in cane blanket properties which may occur in factory milling due to variations in cane variety and level of comminution.

Fig. 6. Roll torque versus compression ratio for experiment and finite element simulation: ---□-- empirical (Loughran, 1990), —◇— simulation (set 1 material parameters), —●— simulation (set 2 material parameters). Set 1 material properties were determined from very low speed (5 and 10mm/min) compression tests on Q96 variety sugar cane. Set 2 material properties were determined by extrapolation to determine the zero-speed (solid matrix only) component from tests performed at higher compression speed (18-71mm/s), using coarser (less finely shredded) cane samples. The two sets are representative of variations in cane blanket properties which may occur in factory milling due to variations in cane variety and level of comminution.

Fig. 7. Predicted energy dissipation versus compression ratio for two-roll simulation (roll surface speed S=150 mm/s, roll diameter D=660 mm):
▨ *bulk plasticity,* ⬚ *frictional sliding,* ▩ *juice flow,* ▧ *seepage induced plasticity*

Fig. 8. Predicted energy dissipation versus roll surface speed for two-roll simulation (nip compression ratio C=2.5, roll diameter D=660 mm):
▨ *bulk plasticity,* ⬚ *frictional sliding,* ▩ *juice flow,* ▧ *seepage induced plasticity*

Fig. 9. Predicted energy dissipation versus feed blanket thickness for two-roll simulation (nip compression ratio C=2.5, roll surface speed S=150 mm/s, roll diameter D=660 mm):
▨ *bulk plasticity,* ⬚ *frictional sliding,* ▩ *juice flow,* ▧ *seepage induced plasticity*

Fig. 10. Deformed finite element meshes for two-roll simulation of blanket thickness as ratios of the reference blanket thickness h_o (nip compression ratio C=2.5, roll diameter D=660 mm): (a) 0.25 h_o, (b) 0.50 h_o, (c) 0.75 h_o, (d) h_o

Tables

Table 1
Two-roll simulation of no-gas saturated thickness of cane blanket h_{ng} (mill compression ratio *C*=2.5, roll diameter *D*=660 mm)

Case	h_{ng}, *mm*	*Roll surface speed (S) mm/s*	*Crushing rate, tonnes cane per hour*	*Roll load, kN*	*Roll torque,* kNm*	*Maximum juice pressure, MPa*
$0.25h_0$	13.1	522	26.46	210	1.8	5.01
$0.50h_0$	26.2	272	26.67	320	4.0	5.07
$0.75h_0$	39.3	190	26.99	385	6.6	4.83
h_0	52.4	150	26.67	420	8.6	4.42

* For a single roll
h_0, reference blanket thickness for the two roll mill

Figures

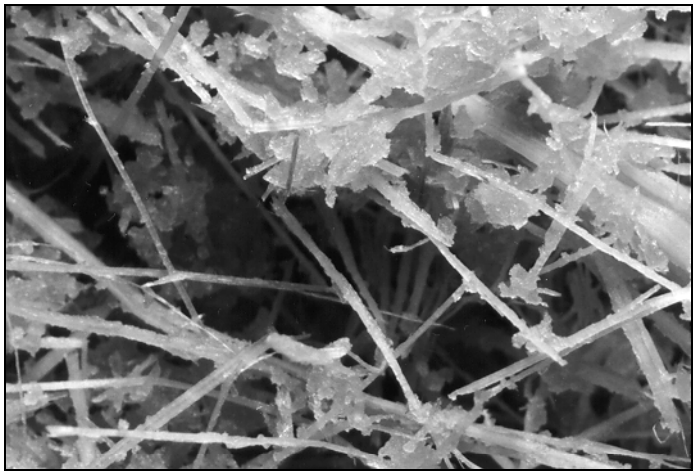

Fig. 1. Structure of shredded sugar cane

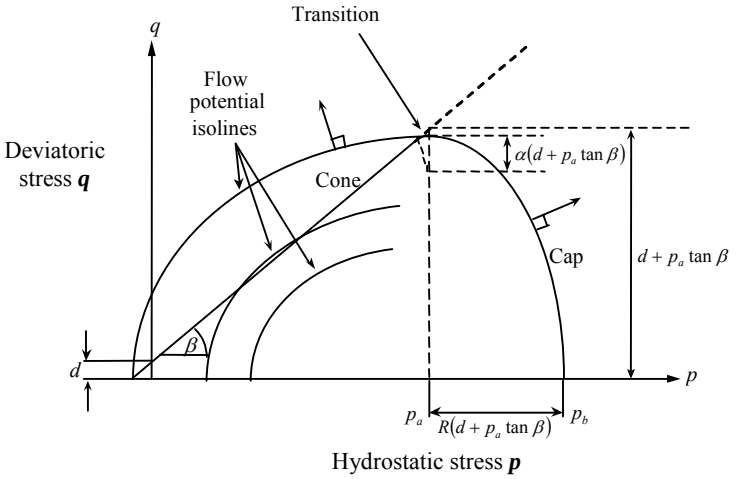

Fig. 2. Yield surface and flow potential for capped Drucker-Prager plasticity: d, cohesion; β, friction angle; α, cap smoothing parameter; R, cap eccentricity; p_a, initial cap size; p_b, current cap size

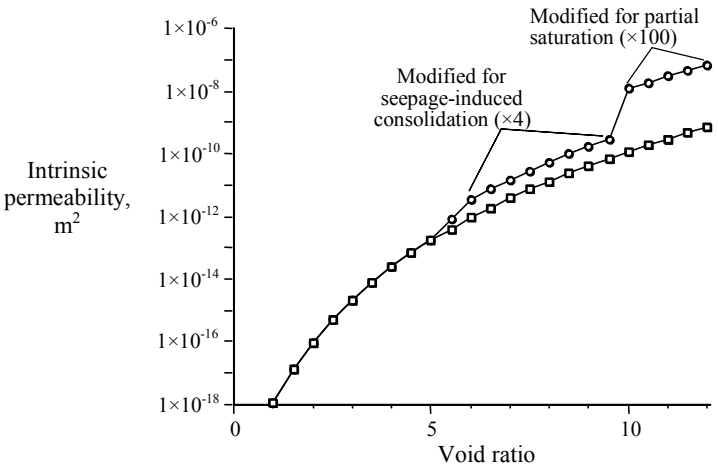

Fig. 3. Permeability response for finite element simulation: ⊟, directly measured; ⊖, modified

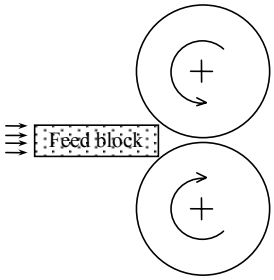

Fig. 4. Schematic two-roll mill

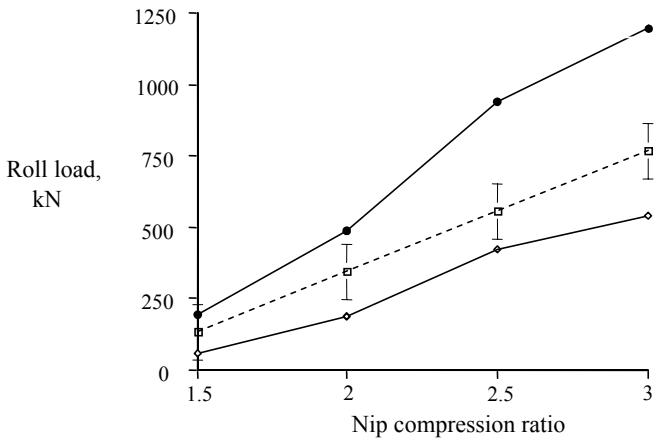

Fig. 5. Roll load versus compression ratio for experiment and finite element simulation: - - -□- - - empirical (Loughran, 1990), —◇— simulation (set 1 material parameters), —●— simulation (set 2 material parameters). Set 1 material properties were determined from very low speed (5 and 10mm/min) compression tests on Q96 variety sugar cane. Set 2 material properties were determined by extrapolation to determine the zero-speed (solid matrix only) component from tests performed at higher compression speed (18-71mm/s), using coarser (less finely shredded) cane samples. The two sets are representative of variations in cane blanket properties which may occur in factory milling due to variations in cane variety and level of comminution.

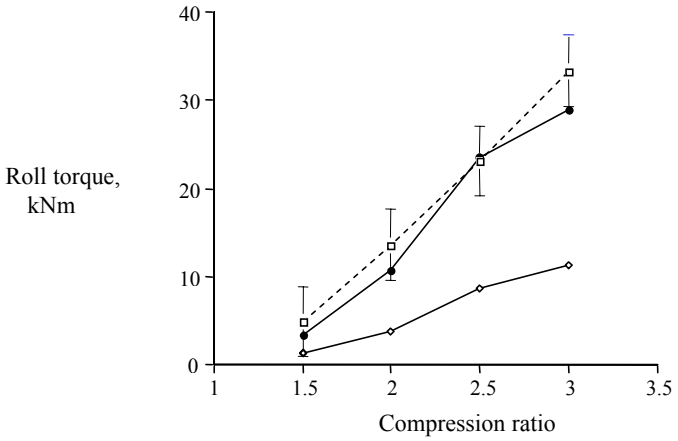

Fig. 6. Roll torque versus compression ratio for experiment and finite element simulation: - - -□- - empirical (Loughran, 1990), —◇— simulation (set 1 material parameters), —●— simulation (set 2 material parameters). Set 1 material properties were determined from very low speed (5 and 10mm/min) compression tests on Q96 variety sugar cane. Set 2 material properties were determined by extrapolation to determine the zero-speed (solid matrix only) component from tests performed at higher compression speed (18-71mm/s), using coarser (less finely shredded) cane samples. The two sets are representative of variations in cane blanket properties which may occur in factory milling due to variations in cane variety and level of comminution.

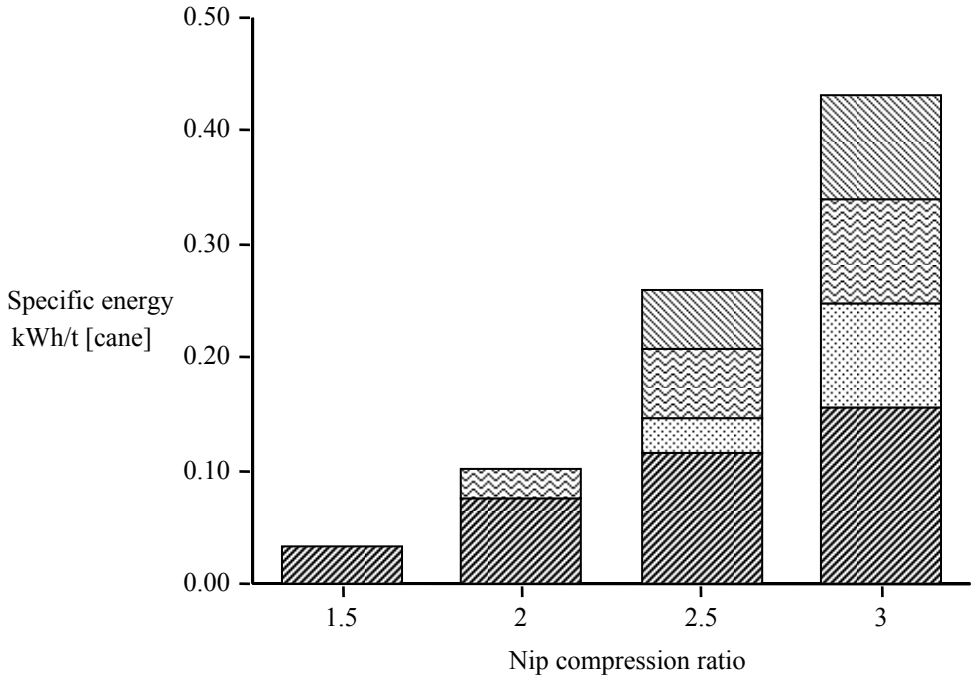

Fig. 7. Predicted energy dissipation versus compression ratio for two-roll simulation (roll surface speed S=150 mm/s, roll diameter D=660 mm):
bulk plasticity, frictional sliding, juice flow, seepage induced plasticity

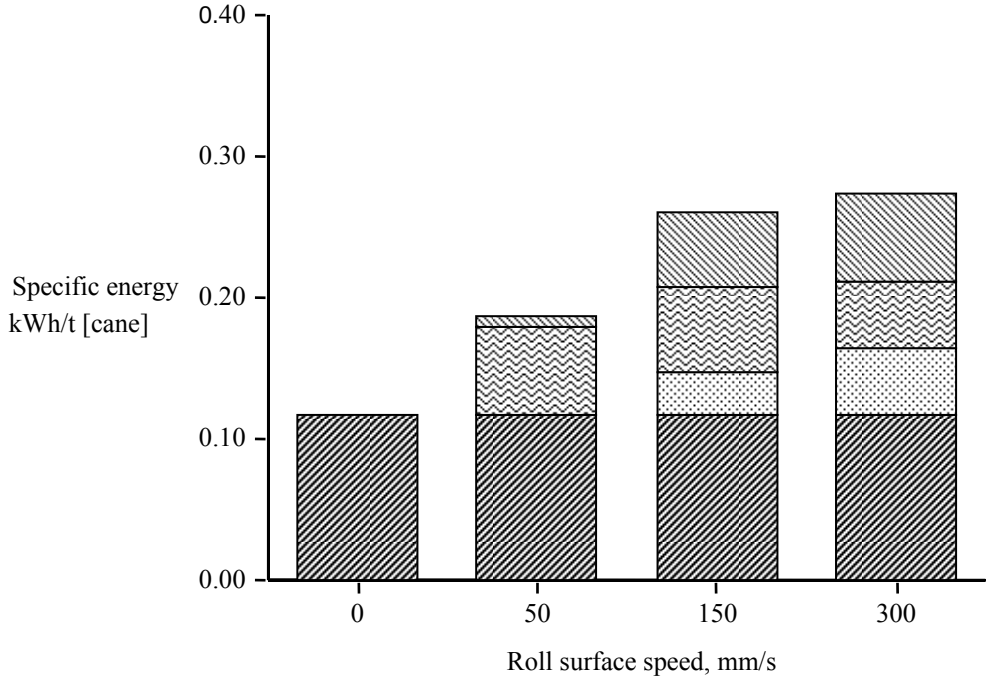

Fig. 8. Predicted energy dissipation versus roll surface speed for two-roll simulation (nip compression ratio C=2.5, roll diameter D=660 mm):
bulk plasticity, frictional sliding, juice flow, seepage induced plasticity

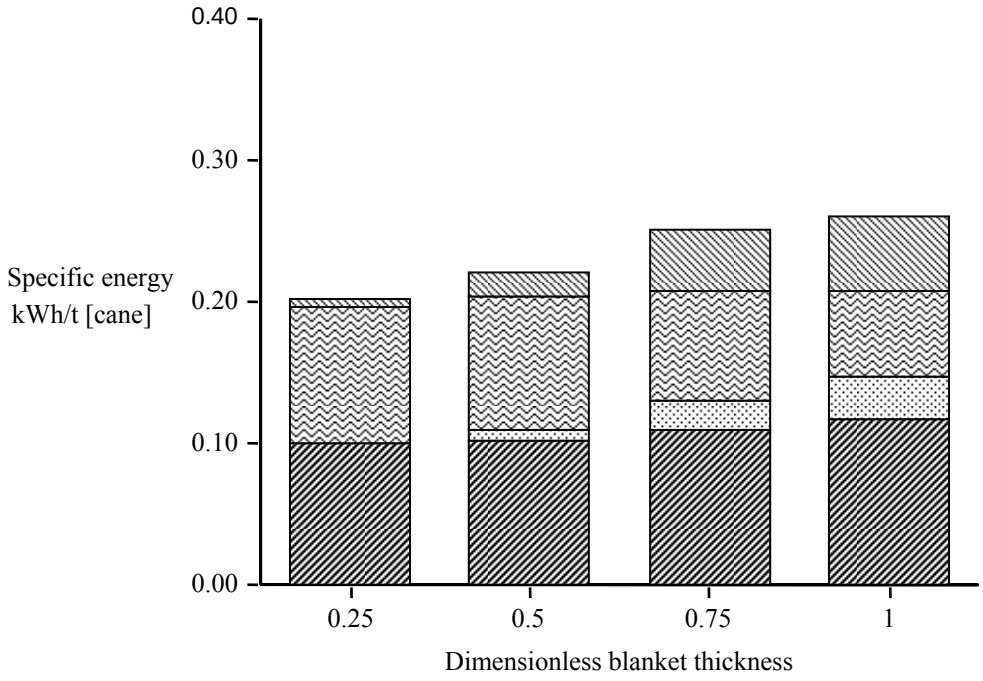

Fig. 9. Predicted energy dissipation versus feed blanket thickness for two-roll simulation (nip compression ratio C=2.5, roll surface speed S=150 mm/s, roll diameter D=660 mm): *bulk plasticity,* *frictional sliding,* *juice flow,* *seepage induced plasticity*

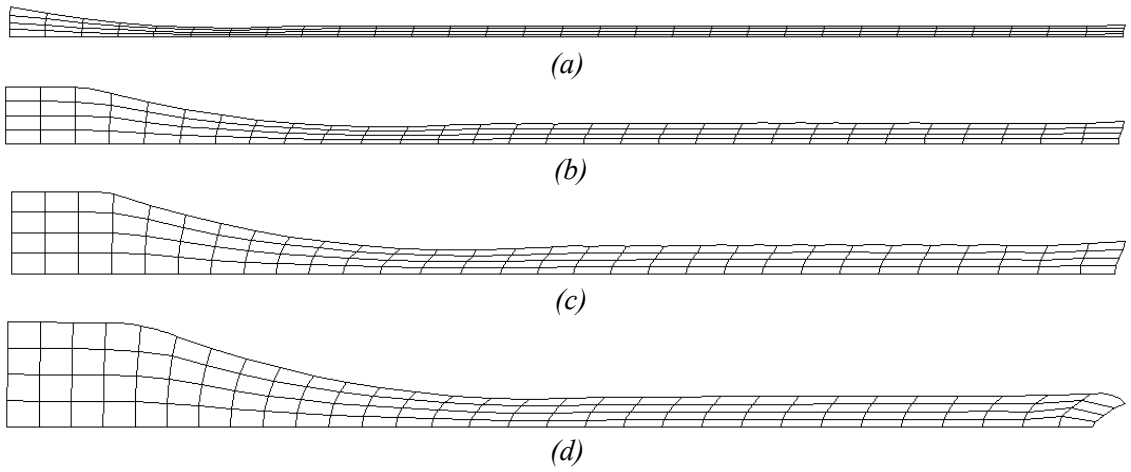

Fig. 10. Deformed finite element meshes for two-roll simulation of blanket thickness as ratios of the reference blanket thickness h_o (nip compression ratio C=2.5, roll diameter D=660 mm): (a) 0.25 h_o, (b) 0.50 h_o, (c) 0.75 h_o, (d) h_o